JACS
JOURNAL OF THE AMERICAN CHEMICAL SOCIETY

Article

pubs.acs.org/JACS

Integration of Porous Coordination Polymers and Gold Nanorods into Core–Shell Mesoscopic Composites toward Light-Induced Molecular Release

Kira Khaletskaya,[†,§] Julien Reboul,[†] Mikhail Meilikhov,[†] Masashi Nakahama,[‡] Stéphane Diring,[†] Masahiko Tsujimoto,[†] Seiji Isoda,[†] Franklin Kim,[†] Ken-ichiro Kamei,[†] Roland A. Fischer,[§] Susumu Kitagawa,*[,†,‡] and Shuhei Furukawa*[,†]

[†]Institute for Integrated Cell-Material Sciences (WPI-iCeMS), Kyoto University, Yoshida, Sakyo-ku, Kyoto 606-8501, Japan

[‡]Department of Synthetic Chemistry and Biological Chemistry, Graduate School of Engineering, Kyoto University, Katsura, Nishikyo-ku, Kyoto 615-8510, Japan

[§]Department of Inorganic Chemistry II, Ruhr University Bochum, Universitätsstrasse 150, 44780 Bochum, Germany

Supporting Information

ABSTRACT: Besides conventional approaches for regulating in-coming molecules for gas storage, separation, or molecular sensing, the control of molecular release from the pores is a prerequisite for extending the range of their application, such as drug delivery. Herein, we report the fabrication of a new porous coordination polymer (PCP)-based composite consisting of a gold nanorod (GNR) used as an optical switch and PCP crystals for controlled molecular release using light irradiation as an external trigger. The delicate core–shell structures of this new platform, composed of an individual GNR core and an aluminum-based PCP shell, were achieved by the selective deposition of an aluminum precursor onto the surface of GNR followed by the replication of the precursor into aluminum-based PCPs. The mesoscopic structure was characterized by electron microscopy, energy dispersive X-ray elemental mapping, and sorption experiments. Combination at the nanoscale of the high storage capacity of PCPs with the photothermal properties of GNRs resulted in the implementation of unique motion-induced molecular release, triggered by the highly efficient conversion of optical energy into heat that occurs when the GNRs are irradiated into their plasmon band. Temporal control of the molecular release was demonstrated with anthracene as a guest molecule and fluorescent probe by means of fluorescence spectroscopy.

INTRODUCTION

Controlled release of chemical substances has proved to be useful in a number of areas including food, pesticide, cosmetic, or medicine.[1−3] In contrast to spontaneous release system from which molecules simply leak, the sophisticated design of materials is required for the development of a controlled or switchable system, in which the release can be initiated or interrupted by responding to external environmental changes, such as temperature,[4] pH,[5] magnetic[6] or electric[7] fields, and ultrasound.[8] In particular, light as an external stimulus is certainly promising because of its facile localizability toward the control of molecular release in spatial and temporal fashions.[9]

Porous coordination polymers (PCPs), a class of crystalline microporous materials composed of metal ions connected to each other by organic ligands, are good candidates for host matrices that transitory but effectively store molecules.[10] This is because of the designability of pores in uniform size and in surface nature for the tunable framework–guest interaction. However, the research on PCPs is totally focused on the control of in-coming molecules into the pores to develop materials for applications in storage,[11] separation,[12] catalysis,[13] and sensing.[14] Regarding the releasing property, a few studies in which the releasing can be initiated by exposing the materials to certain environmental conditions were reported.[15] However, the interruption and restarting of molecular release in a controlled manner is missing. Here we focus our study on the fabrication of a novel PCP platform that temporally controls the release of molecules by light irradiation.

The design of materials takes advantage of photothermal property derived from gold nanorods (GNRs). Upon near-infrared (NIR) light irradiation into the plasmon bands of GNRs, electrons at the excited conduction band relax to the ground state, simultaneously dissipating the resulting excess energy by the conversion of optical energy to heat.[16] Such heat, transferred from the surface of GNRs to the surrounding environment, is highly localized and triggers the release of molecules attached on the gold surface. To date, thermally induced release of the active molecules was achieved either by dissociation of double-stranded DNA molecules into single-stranded DNA,[17] shrinkage of thermo-responsive hydrogel shells,[18] or a morphological change of GNRs.[19] Besides those releasing mechanisms, molecules accommodated into pores can be released by localized heat, which triggers a molecular desorption through the increase of molecular motion. Indeed, the thermal movement of their crystalline lattice as well as the temperature-dependent molecular mobility within their micropores were recently reported.[20] In our approach, this

Received: March 28, 2013
Published: May 14, 2013

   dx.doi.org/10.1021/ja403108x | J. Am. Chem. Soc. 2013, 135, 10998−11005

temperature-dependent molecular motion is exploited to trigger the desorption and diffusion of guest molecules (Scheme 1). Thus, the key for the fabrication is to integrate

Scheme 1. Concept of the Temporally Controlled Guest Release[a]

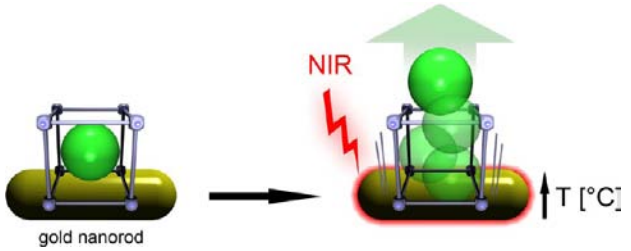

[a]The light-induced molecular release is based on the unique hybrid system where the optical switch GNR is incorporated within PCP.

PCPs and GNRs into core–shell structures, in which the PCP shell is grown in the vicinity of the surface of GNRs. In order to effectively transfer the heat through the whole PCP crystal, the thickness of the PCP shell should be controlled in the mesoscale.

Recent developments in synthetic protocols allowed for the encapsulation of metal nanocrystals within PCP crystals.[21] The synthesized composites displayed performances for catalysis[22] or surface-enhanced Raman scattering.[23] However, heterogeneous structures of metal@PCP composites invariably consisted in a dispersion of a number of metal nanocrystals within large PCP single crystal or crystal aggregates. Very few reports focused on the control of spatial configuration of metal and PCP crystals at the mesoscale[24] and no report, to the best of our knowledge, mentioned the synthesis of nonaggregated core–shell composite, in which individual metal nanocrystals were coated with PCP shells. This is the most likely due to a lack of method to control over the spatial localization of the heterogeneous PCP nucleation. Consequently, a core–shell organization would expand the range of possible applications of metal@PCP composites.

In this work, we show the synthesis of core–shell composites consisted of an individual metal nanorod as a core and well-intergrown PCP crystals as a shell and their potential usage as molecular delivery system. The localized synthesis of PCP only at the surface of GNRs is achieved by coordination replication of alumina to aluminum-based PCP, in which the kinetic coupling between the dissolution of alumina and the crystallization of PCP allowed for the precise localization of PCP nucleation on the targeted environment.[25] Using 1,4-naphthalenedicarboxylic acid H_2(1,4-ndc) as a linker, we convert the core–shell composite of GNR@alumina into GNR@$[Al(OH)(1,4\text{-ndc})]_n$. The resulted composites store high amounts of molecules in the pores of $[Al(OH)(1,4\text{-ndc})]_n$[26] as demonstrated by quartz crystal microbalance (QCM) based sorption experiments. Light-triggered molecular release is confirmed using anthracene as fluorescent probe. While anthracene is strongly confined in the pores of $[Al(OH)(1,4\text{-ndc})]_n$ due to the sufficient host–guest interaction, the heat production from the GNR core under NIR-light irradiation induces the release of anthracene from the pores. We further demonstrate the incorporation of the core–shell composite into biocompartible polymethylglutarimide (PMGI) nanofibers. By the implementation of confocal laser scanning microscopy, the homogeneous distribution of the core–shell composites throughout the nanofibers is clearly observed.

EXPERIMENTAL SECTION

All reagents and solvents were commercially available and used without further purification. Hexadecyltrimethylammonium bromide (99%) (CTAB) and 1,4-ndc (95%) were purchased from Wako Chemicals (Japan). Sodium borohydride, silver nitrate, and L-ascorbic acid were obtained by Nacalai tesque (Japan). Hydrogen tetrachloroaurate (III) hydrate ($HAuCl_4 \cdot 3H_2O$) was purchased from Strem Chemicals (U.S.A.). Thiolated polyethylene glycol (HO-PEG-NH-$CO(CH_2)_2$-SH) with molar weight of 3317 Da was delivered by Rapp Polymer (Germany). Aluminum-tri-*sec*-butoxide (99.99%), aluminum oxide, and anthracene were obtained by Sigma-Aldrich (Japan). The solution of PMGI at 11% in tetrahydrofuran (THF) was purchased from Microchem Corporation (Germany). Sodium dodecyl sulfate (SDS) was purchased from Sigma-Aldrich (Japan). In all experiments deionized water (18.2 MΩ) was used.

Synthesis of CTAB-Stabilized GNRs. CTAB-stabilized GNRs were prepared using the seed-mediated growth method, reported previously.[27] For the seed solution, an aqueous CTAB solution (0.2 M, 5 mL) was first mixed with $HAuCl_4$ solution (0.5 mM, 5 mL) and then with ice-cold $NaBH_4$ solution (0.01 M, 0.6 mL). The reduction of the gold salt resulted in the formation of a brownish yellow solution. Growth solution was prepared by adding of CTAB (0.2 M, 5 mL) to $AgNO_3$ (4 mM, 0.2 mL) and mixing with $HAuCl_4$ (1 mM, 5 mL). A reducing agent in form of ascorbic acid (0.0788 M, 0.07 mL) was then added leading to the formation of a colorless growth solution. Finally, 12 μL of the seed solution was added to the Au^+ stock solution at 30 °C. The reaction was left to proceed for 30 min. The wine-red color of the mixture indicated the formation of the GNRs.

Surface Modification of Gold Nanorods. GNRs were purified by centrifugation (10 000 rpm, 10 min) to remove excess CTAB and were redispersed in 1 mL H_2O. SH-PEG (2 mg) was dissolved in water (200 μL), sonicated for 10 min, and mixed with $NaBH_4$ (20 μL, 0.1 M). The mixture was sonicated for another 15 min to prevent the SH-PEG dimerization (PEG-S-S-PEG). The solutions of GNRs and PEG-SH were mixed under vigorous stirring, sonicated for 30 s and left to react for 5 h. Excess PEG molecules were removed by repeated centrifugation (7000 rpm, 10 min).

Attachment of Amorphous Alumina to the Gold Surface. GNRs were coated with amorphous alumina by hydrolyzing aluminum-tri-*sec*-butoxide in a suspension of nanoparticles. Aluminum-butoxide (7.5 mg) was added in ethanol (1 mL) and sonicated for 1 h to completely dissolve the aluminum source. PEGylated nanorods were washed 2 times with ethanol to remove water and finally resuspended in 1 mL of ethanol. The 100 μL solution of aluminum-butoxide in ethanol was added to 1 mL of GNRs in ethanol strictly under sonication. The two solutions were allowed to sonicate for 1 h. To hydrolyze the aluminum-butoxide into alumina on the surface of GNRs, 200 μL of H_2O was added. The mixture was sonicated for one more hour and washed several times with ethanol to remove alumina, which was not attached to the gold surface.

Conversion of Amorphous Alumina on the Gold Surface into Al-Based PCP. The formation of core–shell composites was performed in the microwave reactor. GNR@alumina was transferred into 1 mL water and mixed with 10 mg of H_2(1,4-ndc). Some drops of nitric acid in water were added to the mixture to adjust the pH value to 2. The mixture was put into a microwave vial equipped with a magnetic stir bar and stirred for 2 min before synthesis. Finally, amorphous alumina on the surface of GNRs was converted into Al-based-PCP, $[Al(OH)(1,4\text{-ndc})]_n$, at 180 °C within 60 s in the microwave reactor (sample labeled GNR@$[Al(OH)(1,4\text{-ndc})]_n$). After cooling down, the core–shell composites were washed several times with *N*,*N*-dimethylformamide (DMF) via slow centrifugation to remove the unconverted linker and empty crystals.

Incorporation of Anthracene into GNR@[Al(OH)(1,4-ndc)]$_n$. The anthracene loading was performed by soaking of dried core–shell

dx.doi.org/10.1021/ja403108x | J. Am. Chem. Soc. 2013, 135, 10998–11005

composites (DMF was exchanged to dichloromethane and core−shell composites were dried overnight at 70 °C under vacuum) in a 20 mM cyclohexane solution of anthracene in a thermomixer at room temperature for 24 h. After insertion of the guest, the core−shell composites were washed by following a procedure to remove the anthracene molecules from the surface of the crystals. After soaking of core−shell composites in the anthracene solution of cyclohexane for 24 h, the composites were centrifuged. The core−shell composites felt to the bottom of container, and the excess of anthracene remained in the supernatant. Then, the composites were moved to the fresh cyclohexane and again centrifuged. This procedure was repeated three times. Finally, the absence of remaining anthracene in the supernatant was confirmed by UV−vis spectroscopy.

Light-Induced Anthracene Release. The sample of core−shell composites with incorporated anthracene molecules was divided into 14 equal parts. In general, seven experiments were performed. Thereby, 2 parts were resuspended in 1 mL cyclohexane each. One sample was then directly irradiated with the Xenon lamp (NIR-light: wavelength = 750 nm) for 1, 5, 10, 15, 30, 60, and 120 min, while another one was left in the solution for the same times without any irradiation in order to assess the passive anthracene release. After each experiment, both samples were centrifuged, and the fluorescence spectra of the supernatants with and without lamp irradiation were recorded and compared to each other. Reference experiments were performed with $[Al(OH)(1,4\text{-ndc})]_n$ loaded with anthracene but without GNRs inside.

Fabrication of Hybrid PMGI Nanofibers Embedding GNR@$[Al(OH)(1,4\text{-ndc})]_n$. For the fabrication of nanofibers the previously reported electrospinning method was used.[28] First, the viscous PMGI solution was mixed with sodiumdodecylsulfate to avoid the formation of undesired beads in fibers. Core−shell composites loaded with anthracene were suspended in 136 μL tetrahydrofuran (THF) and added to 364 μL of 11% v/v PMGI solution. Consequently, the final concentration of the polymer solution was 8% v/v. The polymer solution was loaded into 1 mL syringe with a stainless steel 18-gauge needle connected to a high-voltage supply, and the distance between the needle and the silicon wafer placed with a collector (a microscope glass substrate or a TEM grid) was kept at 10 cm. A voltage of 8 kV vs the silicon wafer with the collector was applied to the needle. Then, nanofibers incorporated with core−shell composites were produced onto the collector by ejecting the polymer solution with a syringe pump at a feeding rate of 0.6 μL/min.

RESULTS AND DISCUSSION

Fabrication of Core−Shell Composite. For a shell we chose the previously reported PCP framework composed of aluminum hydroxide chains and 1,4-ndc linkers $[Al(OH)(1,4\text{-ndc})]_n$.[26] To ensure an accurate localization of the PCP crystal nucleation onto GNRs, the gold nanoparticles were first coated with a hydrated amorphous alumina layer that acted as localized aluminum source (Scheme 2). The alumina-modified nanorods were then used as reactive seeds. Dissolution of the amorphous alumina coating during a microwave treatment in the presence of 1,4-naphthalenedicarboxylate promoted the nucleation of an aluminum-based PCP on the surface of the GNR.

GNRs were first synthesized by applying a seed-mediated growth method.[27] This approach produced high yield of GNRs with an aspect ratio of ∼4 (Figure 1a). UV−vis spectroscopy was used to observe the plasmon resonance band of the GNRs (Figure 2). The transverse plasmon resonance band peak was located near 517 nm, whereas the tunable longitudinal plasmon band was located near 756 nm. The surface of the GNRs was then modified with PEG-SH polymer chains, which act as a coupling agent for a subsequent alumina coating. Because of the affinity of thiol for gold, CTAB bilayer adsorbed onto the gold surface after the synthesis was displaced by the PEG-SH.[29] Surface-functionalized GNRs exhibited high sterical stability

Scheme 2. Schematic Illustration of the Synthesis of GNR@$[Al(OH)(1,4\text{-ndc})]_n$ Core−Shell Composites Capable of Light-Controlled Molecular Release

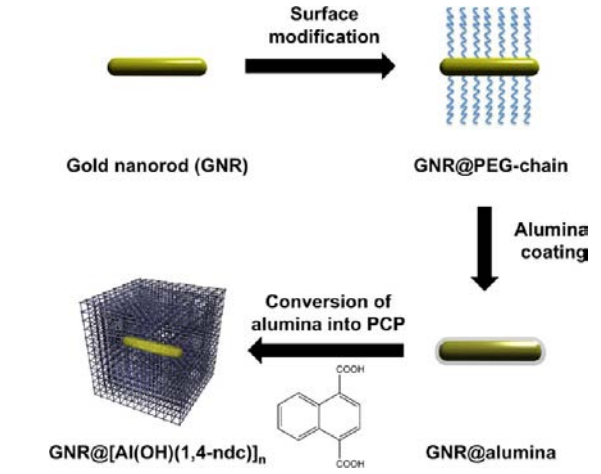

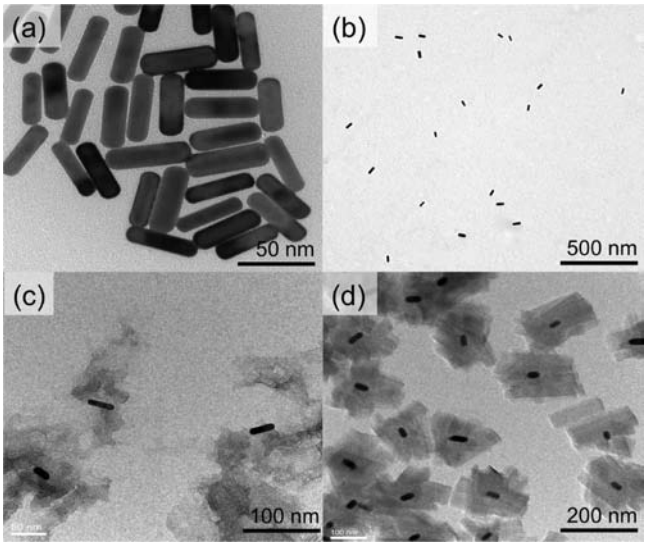

Figure 1. TEM images of (a) CTAB-stabilized GNRs, (b) GNRs after the surface modification with PEG-SH, (c) PEGylated GNRs coated with amorphous alumina, and (d) core−shell composites.

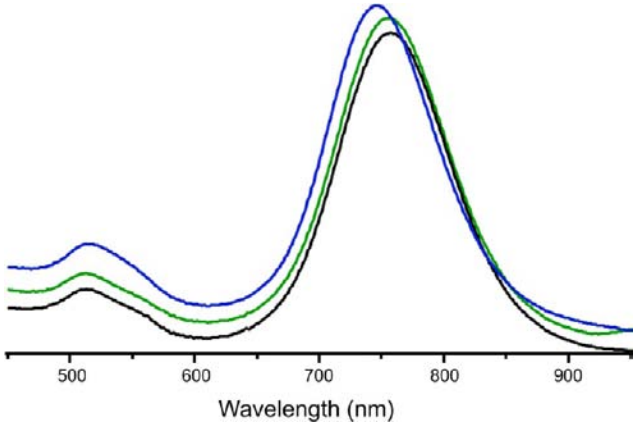

Figure 2. UV−vis spectra of GNR@CTAB (black), of GNR@PEG (green), and GNR@alumina (blue).

dx.doi.org/10.1021/ja403108x | J. Am. Chem. Soc. 2013, 135, 10998−11005

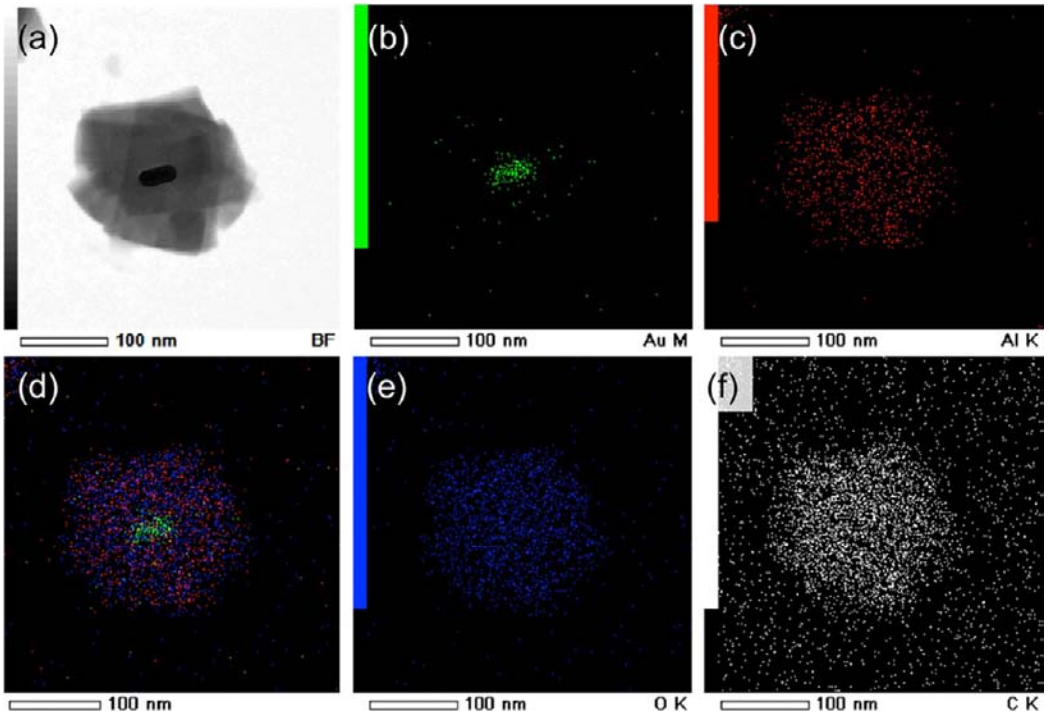

Figure 3. EDX elemental mapping images of single GNR@$[Al(OH)(1,4\text{-ndc})]_n$ core−shell composite. (a) TEM image of composite and elemental mapping images by (b) Au, (c) Al, (d) all merged, (e) O, and (f) C.

and, therefore, remained nonaggregated as observed on the transmission electron microscopy (TEM) images (Figures 1b). The successful PEG-coating was confirmed by X-ray fluorescence spectrometry (XRF) that shows the presence of thiol functions (Table S1). The UV−vis spectrum of the PEG-modified GNRs showed two extinction peaks at 517 and 755 nm (Figure 2). No significant changes in both of plasmon band shapes and positions were observed compared to the CTAB-stabilized GNRs. Change in chemical environment at the gold surface after CTAB exchange by PEG is likely not significant enough to induce a clear shift of the plasmon band position.

An amorphous alumina layer was then deposited onto the gold surface by a sol−gel process. PEGylated GNRs were mixed with a dry ethanolic solution of aluminum-tri-*sec*-butoxide as an aluminum precursor. Mineral polymerization was initiated by the addition of a small amount of water and led to GNRs embedded within a hydrated amorphous alumina matrix. Notably, no well-defined core−shell GNR@alumina nanostructures were observed on TEM pictures (Figures 1c and S1). We believe that the irregular alumina coating observed on these pictures is an artifact originating from the preparation of the TEM grids. Indeed, at room temperature and under the experimental conditions, the amorphous alumina produced in water/ethanol solution is most likely composed of soluble aluminum hydroxide oligomers attached to the PEG chains through the formation of a hydrogen-bonding network between the ethylene oxide units of the PEG chains and the hydroxide groups of the alumina species.[30] The observed irregular alumina coating likely originated from the collapse and further condensation of the soluble alumina species during the drying step of TEM grids preparation. The coverage of the GNR surface by soluble alumina species was further validated by a shift of the surface plasmon band (Figure 2) and energy-dispersive X-ray spectroscopy (EDX) (Figure S2). Though the transverse plasmon band remains almost unchanged, a slight blue shift of the longitudinal plasmon band occurred upon deposition of the alumina layer.

Finally, 1,4-naphthalenedicarboxylic acid linkers were added to the freshly washed GNR/alumina suspension, and the resulting mixture was treated under microwave conditions. Localized PCP nucleation on the GNR surface resulted in the formation of discrete particles with a well-defined core−shell composites (Figures 1d and S3). EDX mapping measured on one core−shell composite (Figures 3) displays signals corresponding to the carbon atoms, which proves the formation of a hybrid shell around the GNRs. Powder X-ray diffraction (PXRD) measurement for the core−shell composites unambiguously reveals the formation of the $[Al(OH)(1,4\text{-ndc})]_n$ phase (Figure S4). This result is confirmed by the analysis in selected-area electron diffraction of the shell that shows a ring-like diffraction pattern reflecting the contribution from $[Al(OH)(1,4\text{-ndc})]_n$ crystallites with a random orientation (Figure S5). The field emission scanning electron microscopy (FESEM) image presented in Figure 4 points out the homogeneity of the sample that is composed of few intergrown PCP nanocrystals aggregated around individual GNRs with a mean size of 300 nm.

Utilization of alumina-modified GNRs as reactive seeds was the key point to precisely controlling the localization of PCP crystallization onto the gold surface. This strategy directly derives from a dissolution−recrystallization process, so-called coordination−replication, which we established in the previous study for the formation of PCP architectures.[25] This process is based on the pseudomorphic replacement of a metal oxide phase that is out of equilibrium by a more stable PCP framework in the presence of multitopic organic ligands. Preservation of the shape and dimension of the parent phase is guaranteed by a precise coupling between kinetics of the metal oxide dissolution and kinetics of PCP crystallization. In the case of GNR@$[Al(OH)(1,4\text{-ndc})]_n$ formation, the alumina species

dx.doi.org/10.1021/ja403108x | *J. Am. Chem. Soc.* 2013, 135, 10998−11005

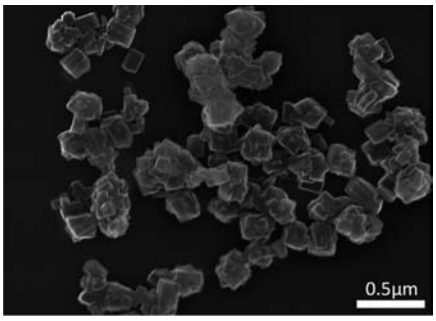

Figure 4. FESEM images of core−shell composites.

attached onto the gold surface act as localized aluminum source. Their dissolution is immediately followed by the fast crystallization of $[Al(OH)(1,4\text{-ndc})]_n$. Surface of GNRs acts as starting point for the PCP heterogeneous nucleation. Noteworthy, local Joule heating resulting from the adsorption of the microwave energy by the conductive GNR most likely also contributes to the promotion of the heterogeneous PCP nucleation. Indeed, the effect of this phenomenon upon heterogeneous PCP nucleation of gold substrates was previously reported.[31]

Temporal Control of Molecular Release Using Light Irradiation. Core−shell composites were then tested as molecular release systems. Anthracene was chosen as a guest model molecule for two main reasons: (1) Anthracene molecules can be strongly stabilized within $[Al(OH)(1,4\text{-ndc})]_n$ PCP pores through both a perfect size matching (on the basis of the crystallographic data and the van der Walls radii of atoms dimensions of the large channels of $[Al(OH)(1,4\text{-ndc})]_n$ are about 7.7 × 7.7 Å, while the in-plane van der Walls dimensions of anthracene are 11.3 × 7.4 Å) and strong $\pi-\pi$ stacking interactions between anthracene and naphthalene moiety at the pore wall. Such an efficient stabilization is critical in order to avoid any leakage of guest molecules. Here we took an advantage of PCPs that enable to stabilize small molecules in the pores through physisorption, without the requirement of the specific chemical modification. (2) Owing to its fluorescence properties in its solubilized state, anthracene can be used as a probe that allows for an easy detection of the molecular release by means of fluorescence spectroscopy measurements.

Athracene incorporation and stabilization within the pore of $[Al(OH)(1,4\text{-ndc})]_n$ were first investigated. Anthracene was loaded into the PCP shell by soaking the composite particles in a 20 mM cyclohexane solution at room temperature for 24 h. The composite materials were first activated by the guest exchange from DMF to dichloromethane followed by a drying process at 70 °C overnight under vacuum. Anthracene loading within the PCP pore was evidenced by means of methanol sorption analysis. Methanol adsorption properties were investigated before and after anthracene loading by environment-controlled quartz crystal microbalance (QCM) technique (Figure 5).[32] All isotherms were measured simultaneously in a six-channel QCM chamber. Adsorption isotherm measured at 25 °C with activated GNR@$[Al(OH)(1,4\text{-ndc})]_n$ composites before anthracene loading displays a type-I behavior, revealing the microporosity of the $[Al(OH)(1,4\text{-ndc})]_n$ framework (black trace).[26] After loading with anthracene, the saturation uptake at P/P_0 = 100% decreased by a factor 2, evidencing the successful incorporation of anthracene guest molecules (blue trace). A

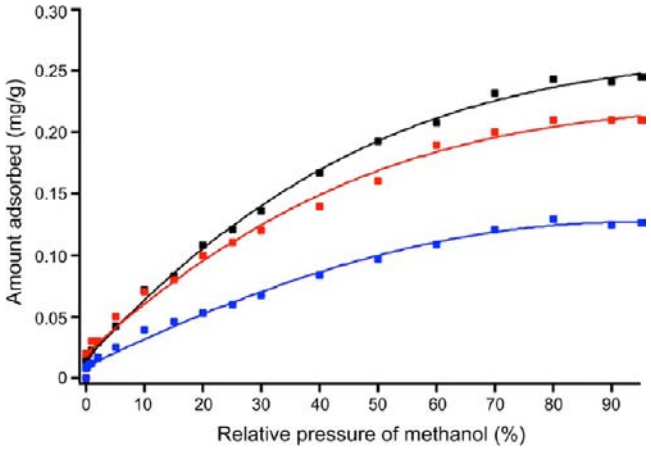

Figure 5. Methanol adsorption isotherms of core−shell composites measured by environment-controlled QCM technique before loading with anthracene (black), after loading (blue), and after release of anthracene (red).

maximum amount of 4 wt % of anthracene adsorbed in the shell was determined by thermogravimetric analysis (TGA; Figures S6).

To demonstrate the photothermal actuation of our molecular release system, NIR irradiation experiments were achieved on both GNR@$[Al(OH)(1,4\text{-ndc})]_n$ composites and $[Al(OH)(1,4\text{-ndc})]_n$ crystals without GNRs as reference. Experiments were performed by using a Xenon light source with an emission wavelength at 750 nm and equipped with an infrared module. Each sample was separated in two batches. During 120 min, one batch was irradiated with NIR in solution, while the other batch was not irradiated in order to evaluate the passive release. Irradiated and nonirradiated samples were centrifuged, and a small aliquot from the supernatant was analyzed by fluorescence spectroscopy at different times of experiment (Figure S7). Figure 6a compares the fluorescence intensities plotted as a function of time for irradiated and nonirradiated core−shell GNR@$[Al(OH)(1,4\text{-ndc})]_n$ composites. Intensity measured in the case of the nonirradiated sample almost did not vary for 120 min, indicating the high stability of the anthracene loaded within the PCP pores and the absence of any leakage. In contrast, a very clear and effective light-induced increase of the fluorescent intensity was observed during the first 60 min in the case of the irradiated sample. The intensity measured after 120 min was 13.4 times higher than for the nonirradiated sample. In order to clarify whether the anthracene escapes from the PCP pores is due to the GNR photoconversion ability or to a possible thermal effect inherent to the NIR irradiation, a similar experiment was then achieved with irradiated and nonirradiated $[Al(OH)(1,4\text{-ndc})]_n$ (without GNRs) as reference (Figure 6b). In this case, fluorescence intensity maxima measured after 120 min for the irradiated sample was only 1.4 times higher than the nonirradiated, indicating the negligible thermal effect of the NIR irradiation upon the anthracene release. Therefore, the burst release of anthracene from the core−shell composites was unambiguously ascribed to the remote heating generated by the GNRs through photothermal conversion. Anthracene light-induced release was also evidenced by solid-state UV−vis measurements (Figure S8) and methanol adsorption QCM measurements (Figure 5).

Figure 5 shows that saturated methanol adsorption capacity measured with GNR@$[Al(OH)(1,4\text{-ndc})]_n$ sample irradiated

dx.doi.org/10.1021/ja403108x | J. Am. Chem. Soc. 2013, 135, 10998−11005

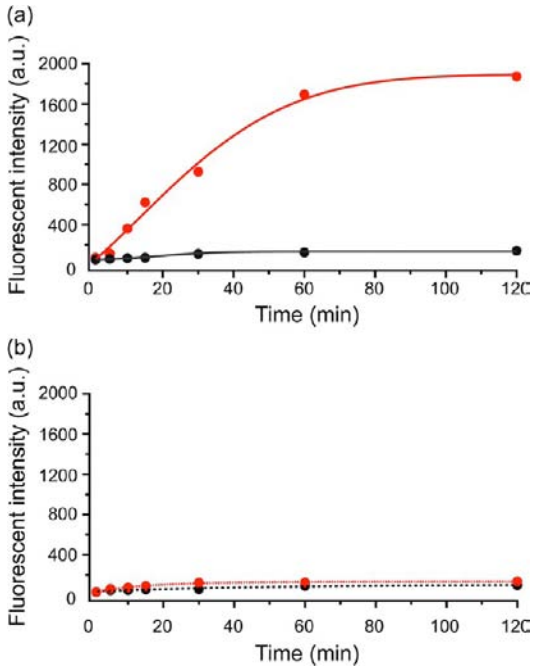

Figure 6. Evaluation of anthracene release from (a) core–shell composites and (b) $[Al(OH)(1,4\text{-ndc})]_n$ crystals without GNRs. The graphs show linear plots for fluorescence intensity maxima of the released anthracene versus time with (red) and without (black) NIR-light irradiation.

for 120 min (red trace) returned to a value close to the saturated methanol adsorption value measured with the sample before anthracene loading (black trace). The lower adsorbed methanol amount observed after NIR-irradiation (35% less than the amount measured with the core–shell composite before anthracene loading) is explained by the presence of a fraction of anthracene that remains trapped within the pores at the end of the irradiation experiment. Indeed, isothermal TGA of the samples before and after NIR-irradiation revealed the presence of 32% of the total amount of loaded anthracene still trapped within the micropores of the PCP shell (Figure S9). These remaining guest molecules most likely correspond to the anthracene molecules the most deeply adsorbed within the PCP pores. As heat generated through photothermal conversion is dependent on the applied NIR irradiation power density,[16] it can be anticipated that the application of higher power densities would further enhance the molecular motion within the hybrid framework and therefore enable the release of the entire amount of loaded anthracene. Importantly, this last result emphasizes the benefit of using PCP crystals as containers when targeting the synthesis of a controlled guest release system. Indeed, in contrast with other porous materials investigated as drug release system, such as porous silica, the efficient guest molecule stabilization provided by PCP micropores consisting of judiciously chosen organic and inorganic building units makes unnecessary any postmodification steps sometimes required to prevent uncontrolled released.[17b]

Spatial Control of Molecular Release by Incorporation of Core–Shell Composite into Nanofibers. GNR@$[Al(OH)(1,4\text{-ndc})]_n$ composites loaded with anthracene were then incorporated into PMGI nanofibers via electrospinning. Though several polymers, such as polyvinylpyrrolidone, polystyrene, or polyacrysonitrile were used for the formation of PCPs/nanofiber composite,[33] we chose PMGI nanofibers, which are biocompatible and easily patternable. The incorporation of the core–shell composites within this organic one-dimensional matrix will allow for the control of their position as well as their integration into bioenvironments.[28]

Electron microscopy (EM) images (Figure 7a,b) clearly display the incorporation of the core–shell composites into

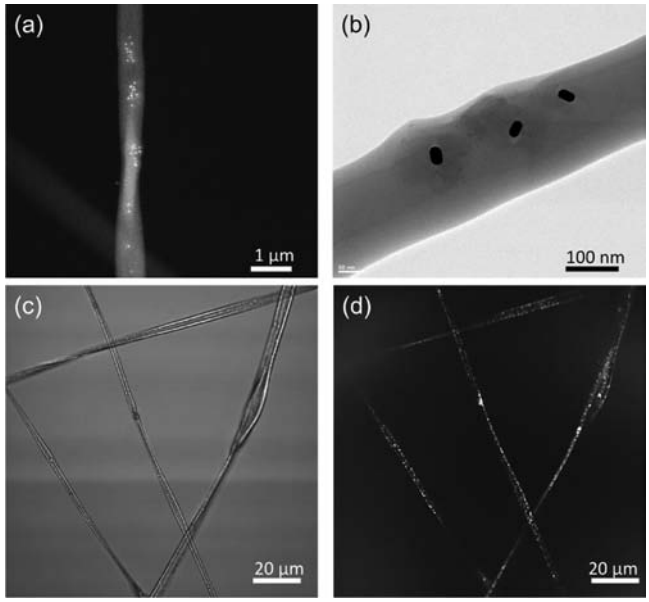

Figure 7. Incorporation of core–shell composites loaded with anthracene into PMGI nanofibers. (a) Annular dark-field scanning transmission electron microscopy and (b) bright-field TEM images of PMGI nanofibers with incorporated core–shell composites. (c) Transmission and (d) CLSM images of the PMGI nanofibers incorporating the core–shell composites loaded with anthracene. Contrast corresponds to the fluorescence intensity from anthracene.

nanofibers with 300 nm to 1 μm thickness. The TEM image (Figure 7b) indicates that the integrity of the core–shell nanostructure remains unchanged even after the incorporation procedure. The confocal laser scanning microscopy (CLSM) images (Figure 7c for transmission and Figure 7d for emission) of the nanofibers incorporating the core–shell composites loaded with anthracene under the excitation at 370 nm also demonstrate the successful incorporation of core–shell composites into PMGI nanofibers. Noteworthy, the homogeneity in size of GNR@$[Al(OH)(1,4\text{-ndc})]_n$ composites and their low degree of aggregation allows for their homogeneous distribution throughout the nanofibers.

■ CONCLUSION

In conclusion, we have developed a strategy for controlling the molecular release from the pores of PCP crystals by combining the loading and unique guest stabilizing ability of PCPs with the photothermal properties of GNRs. In this system, GNRs are individually incorporated within the aggregates of PCP nanocrystals to form well-defined core–shell composites. The photothermal conversion ability of the GNRs acts as an optical switch that enables to remotely release the guest molecules adsorbed within the PCP pores through an increase of molecular mobility. Light-induced release of anthracene demonstrated the efficiency of this new molecular release system. We further demonstrated the method to incorporate the core–shell composites into biocompatible PMGI nano-

dx.doi.org/10.1021/ja403108x | J. Am. Chem. Soc. 2013, 135, 10998–11005

fibers known to be good cell-culture scaffolds.[28a] This system will offer the possibility to spatially control the molecular release and to integrate them into biological systems for future applications in the field of cell biology. It can be anticipated that these PCP-based composites will be used as platform systems for the remote-controlled release of various relevant bioactive molecules to chemically stimulate living cells.

■ ASSOCIATED CONTENT

Ⓢ Supporting Information

Experimental procedures, spectroscopic data, XRF data table, electron microscopy, PXRD and TGA data. This material is available free of charge via the Internet at http://pubs.acs.org.

■ AUTHOR INFORMATION

Corresponding Author

shuhei.furukawa@icems.kyoto-u.ac.jp; kitagawa@icems.kyoto-u.ac.jp

Notes

The authors declare no competing financial interest.

■ ACKNOWLEDGMENTS

This work was supported by ERATO "Kitagawa Integrated Pores Project" of Japan Science and Technology Agency (JST) and Grants-in-Aid for Scientific Research from MEXT (no. 24750201 for Wakate B (J.R.) and no. 24108720 for Priority Area "Coordination Programming" (S.F.)). iCeMS is supported by World Premier International Research Initiative (WPI), MEXT, Japan. K.K. is grateful for support by the Research Department Interfacial Systems Chemistry (IFSC), Ruhr University Bochum.

■ REFERENCES

(1) Zhao, J.; Wilkins, R. M. *J. Agric. Food Chem.* **2003**, *51*, 4023–4028.

(2) Vermonden, T.; Censi, R.; Hennink, W. E. *Chem. Rev.* **2012**, *112*, 2853–2888.

(3) Matthews, D. R.; Lang, D. A.; Burnett, M. A.; Turner, R. C. *Diabetologia* **1983**, *24*, 231–237.

(4) Bae, Y.; Okano, T.; Hsu, R.; Kim, S. *Makromol. Chem., Rapid Commun.* **1987**, *8*, 481–485.

(5) Bae, Y.; Jang, W.-D.; Nishiyama, N.; Fukushima, S.; Kataoka, K. *Mol. Biosyst.* **2005**, *1*, 242.

(6) Lohe, M.; Gedrich, K.; Freudenberg, T.; Kockrick, E.; Dellmann, T.; Kaskel, S. *Chem. Commun.* **2011**, *47*, 3075–3077.

(7) Kwon, I. C.; Bae, Y. H.; Kim, S. W. *Nature* **1991**, *354*, 291.

(8) Kost, J.; Leong, K.; Langer, R. *Proc. Natl. Acad. Sci. U.S.A.* **1989**, *86*, 7663.

(9) Huschka, R.; Neumann, O.; Barhoumi, A.; Halas, N. J. *Nano Lett.* **2010**, *10*, 4117–4122.

(10) (a) Kitagawa, S.; Kitaura, R.; Noro, S. *Angew. Chem., Int. Ed.* **2004**, *43*, 2334–2375. (b) Yaghi, O. M.; O'Keeffe, M.; Ockwig, N. W.; Chae, H. K.; Eddaoudi, M.; Kim, J. *Nature* **2003**, *423*, 705–714. (c) Férey, G.; Mellot-Draznieks, C.; Serre, C.; Millange, F. *Acc. Chem. Res.* **2005**, *38*, 217–225. (d) Dinca, M.; Long, J. R. *Angew. Chem., Int. Ed.* **2008**, *47*, 6766–6779. (e) Morris, R. E.; Wheatley, P. S. *Angew. Chem., Int. Ed.* **2008**, *47*, 4966–4981. (f) Zacher, D.; Shekhah, O.; Wöll, C.; Fischer, R. A. *Chem. Soc. Rev.* **2009**, *38*, 1418–1429. (g) Cohen, S. M. *Chem. Rev.* **2012**, *112*, 970–1000.

(11) (a) Kondo, M.; Yoshitomi, T.; Seki, K.; Matsuzaka, H.; Kitagawa, S. *Angew. Chem., Int. Ed.* **1997**, *36*, 1725–1727. (b) Li, H.; Eddaoudi, M.; O'Keeffe, M.; Yaghi, O. M. *Nature* **1999**, *402*, 276–279. (c) Sumida, K.; Rogow, D. L.; Mason, J. A.; McDonald, T. M.; Bloch, E. D.; Herm, Z. R.; Bae, T.-H.; Long, J. R. *Chem. Rev.* **2012**, *112*, 724–781. (d) Vaidhyanathan, R.; Iremonger, S. S.; Shimizu, G. K. H.; Boyd, P. G.; Alavi, S.; Woo, T. K. *Science* **2010**, *330*, 650–653.

(12) (a) Li, J.-R.; Kuppler, R. J.; Zhou, H.-C. *Chem. Soc. Rev.* **2009**, *38*, 1477–1504. (b) Wang, B.; Côté, A. P.; Furukawa, H.; O'Keeffe, M.; Yaghi, O. M. *Nature* **2008**, *453*, 207–211. (c) Alaerts, L.; Kirschhock, C. E. A.; Maes, M.; van der Veen, M. A.; Finsy, V.; Depla, A.; Martens, J. A.; Baron, G. V.; Jacobs, P. A.; Denayer, J. F. M.; De Vos, D. E. *Angew. Chem., Int. Ed.* **2007**, *46*, 4293–4297. (d) Southon, P. D.; Price, D. J.; Nielsen, P. K.; McKenzie, C. J.; Kepert, C. J. *J. Am. Chem. Soc.* **2011**, *133*, 10885–10891.

(13) (a) Fujita, M.; Know, Y. J.; Washizu, S.; Ogura, K. *J. Am. Chem. Soc.* **1994**, *116*, 1151–1152. (b) Lee, J. Y.; Farha, O. K.; Roberts, J.; Scheidt, K. A.; Nguyen, S. T.; Hupp, J. T. *Chem. Soc. Rev.* **2009**, *38*, 1450–1459. (c) Corma, A.; García, H.; i Xamena, F. X. L. *Chem. Rev.* **2010**, *110*, 4606–4655.

(14) (a) Takashima, Y.; Martínez, V. M.; Furukawa, S.; Kondo, M.; Shimomura, S.; Uehara, H.; Nakahama, M.; Sugimoto, K.; Kitagawa, S. *Nat. Commun.* **2011**, *2*, 168. (b) Kreno, L. E.; Leong, K.; Farha, O. K.; Allendorf, M.; Van Duyne, R. P.; Hupp, J. T. *Chem. Rev.* **2012**, *112*, 1105–1125. (c) Shustova, N. B.; McCarthy, B. D.; Dinca, M. *J. Am. Chem. Soc.* **2011**, *133*, 20126–20129.

(15) (a) Horcajada, P.; Serre, C.; Vallet-Regí, M.; Sebban, M.; Taulelle, F.; Ferey, G. *Angew. Chem., Int. Ed.* **2006**, *45*, 5974. (b) McKinlay, A. C.; Bo, X.; Wragg, D. S.; Wheatley, P. S.; Megson, I. L.; Morris, R. E. *J. Am. Chem. Soc.* **2008**, *130*, 10440–10444. (c) Tsotalas, M.; Hejcik, P.; Sumida, K.; Kalay, Z.; Furukawa, S.; Kitagawa, S. *J. Am. Chem. Soc.* **2013**, *135*, 4608–4611.

(16) Lee, S. E.; Liu, G. L.; Kim, F.; Lee, L. P. *Nano Lett.* **2009**, *9*, 562–570.

(17) (a) Yamashita, S.; Fukushima, H.; Akiyama, Y.; Niidome, Y.; Mori, T.; Katayama, Y.; Niidome, T. *Bioorg. Med. Chem.* **2011**, *19*, 2130–2135. (b) Yang, H.; Liu, X.; Liu, Z.; Pu, F.; Ren, J.; Qu, X. *Adv. Mater.* **2012**, *24*, 2890–2895.

(18) Kawano, T.; Niidome, Y.; Mori, T.; Katayama, Y.; Niidome, T. *Bioconjugate Chem.* **2009**, *20*, 209–212.

(19) (a) Takahashi, H.; Niidome, Y.; Yamada, S. *Chem. Commun.* **2005**, 2247–2249. (b) Chen, C.; Lin, Y.; Wang, C.; Tzeng, H.; Wu, C.; Chen, Y.; Chen, C.; Chen, L.; Wu, Y. *J. Am. Chem. Soc.* **2006**, *128*, 3709–3715.

(20) (a) Han, S. S.; Goddard, W. A. *J. Phys. Chem. C* **2007**, *111*, 15185–15191. (b) Stallmach, F.; Gröger, S.; Künzel, V.; Kärger, J.; Yaghi, O. M.; Hesse, M.; Müller, U. *Angew. Chem., Int. Ed.* **2006**, *45*, 2123–2126.

(21) Meilikhov, M.; Yusenko, K.; Esken, D.; Turner, S.; Van Tendeloo, G.; Fischer, R. A. *Eur. J. Inorg. Chem.* **2010**, 3701–3714.

(22) Hermes, S.; Schröter, M.-K.; Schmid, R.; Khodeir, L.; Muhler, M.; Tissler, A.; Fischer, R. W.; Fischer, R. A. *Angew. Chem., Int. Ed.* **2005**, *44*, 6237–6241.

(23) Sugikawa, K.; Furukawa, Y.; Sada, K. *Chem. Mater.* **2011**, *23*, 3132–3134.

(24) (a) Kuo, C.-H.; Tang, Y.; Chou, L.-Y.; Sneed, B. T.; Brodsky, C. N.; Zhao, Z.; Tsung, C. K. *J. Am. Chem. Soc.* **2012**, *134*, 14345. (b) Falcaro, P.; Hill, A. J.; Nairn, K. M.; Jasieniak, J.; Mardel, J. I.; Bastow, T. J.; Mayo, S. C.; Gimona, M.; Gomez, D.; Whitfield, H. J.; Riccò, R.; Patelli, A.; Marmiroli, B.; Amenitsch, H.; Colson, T.; Villanova, L.; Buso, D. *Nat. Commun.* **2011**, *2*, 237. (c) Lu, G.; Li, S.; Guo, Z.; Farha, O. K.; Hauser, B. G.; Qi, X.; Wang, Y.; Wang, X.; Han, S.; Liu, X.; DuChene, J. S.; Zhang, H.; Zhang, Q.; Chen, X.; Ma, J.; Loo, S. C. J.; Wei, W. D.; Yang, Y.; Hupp, J. T.; Huo, F. *Nat. Chem.* **2012**, *4*, 310–316.

(25) Reboul, J.; Furukawa, S.; Horike, N.; Tsotsalas, M.; Hirai, K.; Uehara, H.; Kondo, M.; Louvain, N.; Sakata, O.; Kitagawa, S. *Nat. Mater.* **2012**, *11*, 717–723.

(26) Comotti, A.; Bracco, S.; Sozzani, P.; Horike, S.; Matsuda, R.; Chen, J.; Takata, M.; Kubota, Y.; Kitagawa, S. *J. Am. Chem. Soc.* **2008**, *130*, 13664.

(27) (a) Jana, N.; Gearheart, L.; Murphy, C. J. *Adv. Mater.* **2001**, *13*, 1389. (b) Nikoobakht, B.; El-Sayed, M. A. *Chem. Mater.* **2003**, *15*, 1957–1962.

(28) (a) Liu, L.; Yuan, Q.; Shi, J.; Li, X.; Jung, D.; Yamauchi, K.; Nakatsuji, N.; Kamei, K.; Chen, Y. *Biotechnol. Lett.* **2012**, *34*, 1951−1957. (b) Teo, W. E.; Ramakrishna, S. *Nanotechnology* **2006**, *17*, 89−106.
(29) Liao, H. W.; Hafner, J. H. *Chem. Mater.* **2005**, *17*, 4636−4641.
(30) (a) Yoldas, B. E. *J. Appl. Chem. Biotechnol.* **1973**, *23*, 803. (b) Cai, W.; Yu, J.; Jaroniec, M. *J. Mater. Chem.* **2001**, *21*, 9066−9072.
(31) (a) Hecht, E. *Optics*, 3rd ed.; Addison Wesley Longman, Inc.: New York, 1998. (b) Yoo, Y.; Jeong, H. K. *Chem. Commun.* **2008**, 2441−2443.
(32) Uehara, H.; Diring, S.; Furukawa, S.; Kalay, Z.; Tsotsalas, M.; Nakahama, M.; Hirai, K.; Kondo, M.; Sakata, O.; Kitagawa, S. *J. Am. Chem. Soc.* **2011**, *133*, 11932−11935.
(33) (a) Ostermann, R.; Cravillon, J.; Weidmann, C.; Wiebcke, M.; Smarsly, B. M. *Chem. Commun.* **2011**, *47*, 442−444. (b) Rose, M.; Böhringer, B.; Jolly, M.; Fischer, R.; Kaskel, S. *Adv. Eng. Mater.* **2011**, *4*, 356−360.